

# Transformation-Invariant Network for Few-Shot Object Detection in Remote Sensing Images

Nanqing Liu, Xun Xu, Turgay Celik, Zongxin Gan, Heng-Chao Li

**Abstract**—Object detection in remote sensing images relies on a large amount of labeled data for training. The growing new categories and class imbalance render exhaustive annotation non-scalable. Few-shot object detection (FSOD) tackles this issue by meta-learning on seen base classes and then fine-tuning on novel classes with few labeled samples. However, the object’s scale and orientation variations are particularly large in remote sensing images, thus posing challenges to existing few-shot object detection methods. To tackle these challenges, we first propose to integrate a feature pyramid network and use prototype features to highlight query features to improve upon existing FSOD methods. We refer to the modified FSOD as a Strong Baseline which is demonstrated to perform significantly better than the original baselines. To improve the robustness of orientation variation, we further propose a transformation-invariant network (TINet) to allow the network to be invariant to geometric transformations. Extensive experiments on three widely used remote sensing object detection datasets, i.e., NWPU VHR-10.v2, DIOR, and HRRSD demonstrated the effectiveness of the proposed method. Finally, we reproduced multiple FSOD methods for remote sensing images to create an extensive benchmark for follow-up works.

**Index Terms**—Remote sensing images, few-shot learning, meta-learning, object detection, transformation invariance.

## I. INTRODUCTION

Optical remote sensing analyzes images captured by satellites and aerial vehicles. There are huge values for analyzing these remote sensing images (RSIs), e.g. monitoring climate change, detecting forest fires, and commercial analytics. Detecting natural and man-made objects from RSIs is the most critical capability that supports the above analytic tasks. The state-of-the-art approaches toward object detection in RSIs [1, 2, 3, 4] employ a deep learning-based paradigm that requires a substantial amount of labeled data for supervised training. Nevertheless, there are several key challenges that prohibit standard supervised object detection training from scaling up. First, the existing object detection approaches often detect the objects from the seen semantic categories while the potential objects of interest are always non-exhaustive. When new categories of objects emerge, collecting enough labeled

training data for novel categories is prohibitively expensive. Moreover, semantic objects in RSIs are highly imbalanced, as evidenced by the frequency of objects in the DIOR dataset [5] in Fig. 1 (a). This observation suggests that even if exhaustive annotation might be possible, collecting enough training examples for the minority classes is non-trivial which again motivates us to explore learning from a few labeled examples.

To address the challenges in data efficiency, we approach from a few-shot object detection (FSOD) paradigm [6]. For object detection on natural semantic images, FSOD has been extensively studied following a meta-learning approach. However, it is suboptimal to directly apply existing FSOD methods on RSIs due to the following two reasons. First, the size of objects varies substantially across images, detecting objects at a fixed resolution is limited in generalizing to objects of large size variation. Second, the orientation in RSIs is more diverse than objects in natural images, since the camera is positioned in a nadir view and arbitrary rotation in the XOY plane is allowed. In comparison, natural semantic images are often captured by cameras sitting upright, thus having less diverse poses.

In this paper, we propose a meta-learning-based few-shot object detection framework to address the above challenges. First, we build the object detection framework based on Faster-RCNN [7]. Previous meta-learning approaches [6] [8] simply adopted a single-level feature of the backbone to generate proposals. Therefore, to adapt to scale variation in RSIs, we introduce the feature pyramid network (FPN) [9] to the meta-learning approach. We further propose to highlight query feature maps with support prototype features through depth-wise convolution. The above modifications to the existing meta-learning-based FSOD method are demonstrated to substantially improve the performance of FSOD on RSIs. We refer to the modified FSOD method as the Strong Baseline throughout this paper.

In addition to proposing the Strong Baseline model, we further tackle the challenge brought by large orientation variation by introducing a transformation-invariant network (TINet). Specifically, we observe that the Strong Baseline cannot adapt well to image transformations such as flipping and rotation. Hence, the query image and its transformed version are used as the input of the shared backbone and FPN simultaneously. Then, we aggregate the support feature with the query feature of the original image and transformed image, which are produced by RoI Align through the region proposals. Consistency regularization is applied to a one-to-one correspondence between the predicted boxes in the original and the transformed images. With these operations, the TINet is forced to produce

This work was supported in part by the National Natural Science Foundation of China under Grant 62271418, and in part by the Natural Science Foundation of Sichuan Province under Grant 23NSFSC0058.

Nanqing Liu (lansing163@163.com), Turgay Celik (celikturgay@gmail.com), Zongxin Gan (gccxeon@my.swjtu.edu.cn), Heng-Chao Li (lihengchao\_78@163.com) are with the School of Information Science and Technology, Southwest Jiaotong University, Chengdu, China. Turgay Celik is also with the School of Electrical and Information Engineering, University of the Witwatersrand, Johannesburg, South Africa.

Xun Xu (xux@i2r.astar.edu.sg) is with I2R, A-STAR, Singapore 138632, and also with the School of Electronic and Information Engineering, South China University of Technology, Guangzhou 510640, China.

Manuscript revised March 14, 2023.

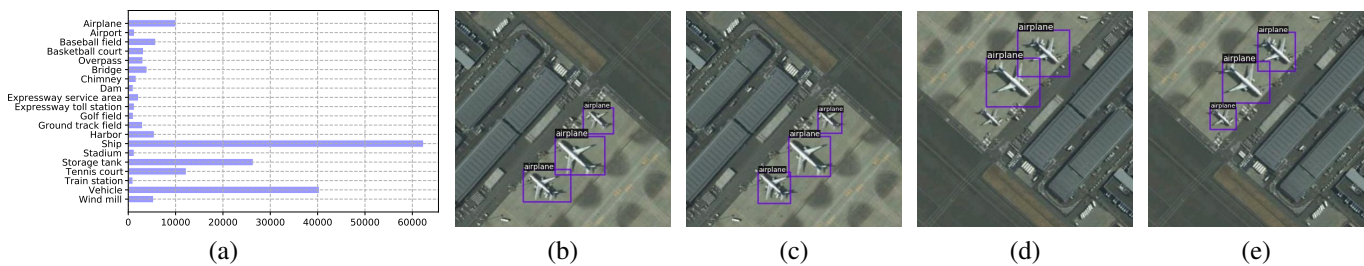


Fig. 1. (a) Number of object instances per class in the DIOR dataset. (b-e) Comparison of the detection results of the Strong Baseline and TINet. (b) Detection results of the Strong Baseline on the original image. (c) Detection results of TINet on the original image. (d) Detection results of the Strong Baseline on the diagonally flipped image. (e) Detection results of TINet on the diagonally flipped image.

consistent predictions on unlabeled images agnostic to camera poses. Therefore, TINet can better identify objects with more diverse orientations. In Fig. 1, we show prediction results of the Strong Baseline and TINet for different inputs. TINet adapts well to the perturbations caused by the transformed images. However, the Strong Baseline failed to locate all the planes, and the localization is less accurate.

To evaluate our proposed model, we conduct extensive experiments on the DIOR [5], HRRSD [10] and NWPU VHR-10.v2 [11] datasets. The proposed TINet achieved the state-of-the-art few-shot object detection performance on all the above datasets. The main contributions of this paper are summarized as follows:

- Motivated by the large-scale variation, we proposed a Strong Baseline few-shot object detection method, which incorporates an FPN and uses  $1 \times 1$  depth-wise convolution to aggregate query and support features. With these operations, the Strong Baseline improves significantly from previous meta-learning FSOD approaches.
- We propose a transformation-invariant network (TINet) based on the Strong Baseline to account for the large orientation variation. TINet only requires adding additional consistency losses between the classification and regression outputs of original and transformed images.
- We reproduced multiple generic FSOD methods for FSOD on RSIs and create an extensive benchmark for follow-up works on FSOD on RSIs. These reproduced generic methods exhibit strong performance even compared with recent FSOD methods dedicated to RSIs.

## II. RELATED WORKS

### A. Object Detection in Remote Sensing Images

Objects in remote sensing images have the following two main characteristics: a large diversity in the object size and orientation. To solve the challenge of scale diversity, Cheng et al. [12] proposed a cross-scale feature fusion (CSFF) strategy to aggregate feature maps from different scales, which results in single-level features containing multiscale receptive fields. [13] constructed a more representative feature pyramid network and selective gate to adapt to large-scale diversity and suppress noise. Wang et al. [14] adopted a feature pyramid structure and atrous convolution with different rates to fuse the context feature information in multiscale features. Ma et al. [15] proposed a feature split-and-merge (FSM) module

to highlight the features of small objects in the shallow feature map. Liu et al. [2] treated the bounding box regression task as a classification task and then used the gather loss and focus loss to obtain a sharper distribution of the bounding boxes. To solve the rotation angle variation, a series of methods for arbitrarily oriented object detection have emerged. Han et al. [16] adopted active rotating filters to encode the orientation information and then produced orientation-sensitive and orientation-invariant features to alleviate the inconsistency between the classification score and the localization accuracy. CSL [17] and DCL [3] were proposed to use a classification label to encode the angle instead of a regression value to solve the problem of discontinuous boundaries, which is directly caused by angular periodicity. Ming et al. [4] proposed transforming the box regression task into an optimal matching process to eliminate the ambiguous representation of the bounding box. The methods mentioned above are all fully supervised. However, this paper focuses on the few-shot setting with a limited dataset, which is more of a challenge.

### B. Few-shot Object Detection

Few-shot Object Detection is categorized into meta-learning and transfer-learning-based approaches. Meta-learning-based approaches [6, 18, 19, 8, 20, 21] extract knowledge that can be generalized across various tasks by learning to learn. FSRW [19] first proposes to extract a global support feature vector to indicate the relevance of the meta-features. Some following works [6, 8, 20] extend this approach to a two-stage network (Faster-RCNN) to substantially improve the accuracy. Transfer-learning-based approaches utilize a simple two-phase approach, which is first trained on the instances of base categories and then fine-tuned on a small number of base and novel samples. To make the fine-tuning processing more effective, TFA [22] uses a classifier based on cosine similarity to fine-tune the last layer of Faster-RCNN. Based on TFA, FSCE [23] introduced contrastive learning to ease misclassification issues. MPSR [24] was proposed to compensate for the lack of positive samples using data augmentation. DeFCRN [25] and CFA [26] improved network performance from the perspective of loss gradients. Compared with few-shot object detection on natural semantic images, object detection in RSIs is subject to additional challenges in more diverse scale and orientation variations. This motivates research into few-shot object detection for RSIs.

### C. Few-shot Object Detection in Remote Sensing Images

Compared with natural semantic images, the size and orientation of objects are more diverse in RSIs. In light of these challenges, most existing works adapt FSOD to RSIs by introducing richer feature extraction modules [27, 28, 29, 30, 31]. In addition to this, some work addresses this problem from other perspectives. For example, Cheng et al. [32] proposed a prototype-guided RPN that injects the information of the support features into the candidate box scores to guide a better generation of the region proposals. Zhang et al. [33] adopted the oriented augmentation of the support feature to alleviate the large diversity in object orientation. In contrast to the existing approaches, we first propose to include an FPN and depth-wise convolution to strengthen the network’s ability to detect objects of diverse scales. To account for a more diverse orientation, we propose a transformation-invariant network to encourage the model to be agnostic to transformation applied to input images.

### D. Transformation Invariant Learning

Transformation invariant learning applies perturbations to an input image  $x$  to obtain  $x'$  and minimizes the difference between the output predictions  $f(x)$  and  $f(x')$ . It is widely adopted in semi-supervised learning [34, 35, 36, 37, 38, 39] and weakly supervised learning [40, 41, 42]. In the area of FSOD, TIP [21] introduces consistency regularization on predictions from various transformed images. However, it only considers classification consistency between two augmentations, so it can only use non-geometric transformation methods (Gaussian noise and cutout) to input images. For remote sensing object detection tasks, regression consistency enforces the spatial locations to be consistent and should also be considered. Different from the above methods, our method incorporates this idea into FSOD in RSIs and verifies the influence of the different transformations and regularizations on the results. It is obvious that our method is the first attempt to address the obstacle of transformed variations in RSIs under few-shot settings.

## III. PROPOSED METHODS

### A. Problem setting

As in various previous works [6][8][19], we follow the standard problem settings of meta-learning-based FSOD in our paper. Specifically, the required data can be divided into two sets of categories,  $\mathcal{C}_{\text{base}}$  and  $\mathcal{C}_{\text{novel}}$ , where  $\mathcal{C}_{\text{base}} \cap \mathcal{C}_{\text{novel}} = \emptyset$ . The few-shot object detector aims at detecting objects of  $\mathcal{C}_{\text{base}} \cup \mathcal{C}_{\text{novel}}$  by learning from a base dataset  $\mathcal{D}_{\text{base}}$  with abundant annotated objects of  $\mathcal{C}_{\text{base}}$  and a novel dataset  $\mathcal{D}_{\text{novel}}$  with very few annotated objects of  $\mathcal{C}_{\text{novel}}$ . In the task of  $K$ -shot object detection, there are exactly  $K$  annotated objects for each novel class in  $\mathcal{D}_{\text{novel}}$ . For the meta-learning approaches, the detector is trained in two phases, i.e., base training and few-shot fine-tuning. In the first phase, the init model  $\mathcal{M}_{\text{init}}$  is trained to base model  $\mathcal{M}_{\text{base}}$  only using base dataset  $\mathcal{D}_{\text{base}}$ . An episodic training scheme is applied, where each of the  $E$  episodes mimics the  $N$ -way  $K$ -shot setting. In each episode  $e$ ,

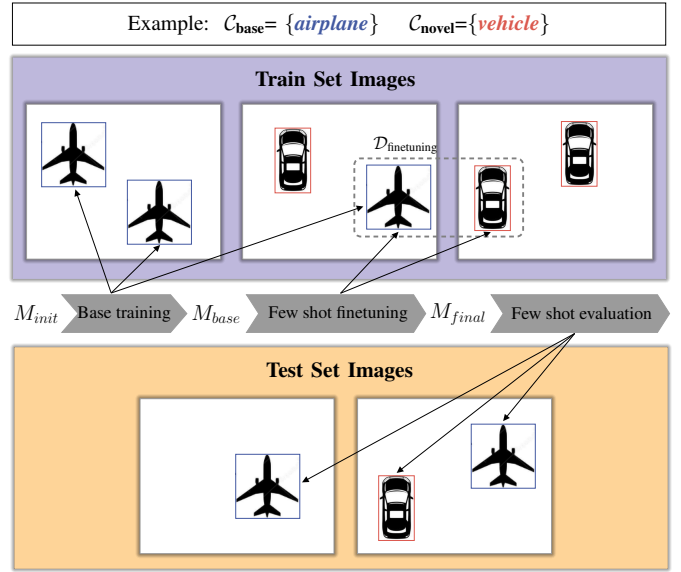


Fig. 2. General idea of few-shot object detection. The training processing can be divided into two phases (base training and few-shot finetuning). In base training, the model  $\mathcal{M}_{\text{init}}$  is trained on base classes, resulting in  $\mathcal{M}_{\text{base}}$ . Then  $\mathcal{M}_{\text{base}}$  can be transferred to  $\mathcal{M}_{\text{final}}$  through fine-tuning on  $\mathcal{D}_{\text{finertuning}}$ , which includes  $K$  samples from each of the novel and base category. In the phase of evaluation, the  $\mathcal{M}_{\text{final}}$  is applied to all the objects in the test set, which includes both novel and base classes.

the model is trained on  $N$  training examples of  $N$  categories on a random subset  $\mathcal{D}_{\text{meta}}^e \subset \mathcal{D}_{\text{base}}$ ,  $|\mathcal{D}_{\text{meta}}^e| = K \cdot N$ . Then, in the few-shot fine-tuning phase, the base model  $\mathcal{M}_{\text{base}}$  also adopts the same episodic training scheme as in the first phase, resulting in the final model  $\mathcal{M}_{\text{final}}$ . Different from the dataset  $\mathcal{D}_{\text{base}}$ , the fine-tuning dataset  $\mathcal{D}_{\text{finertuning}}$  contains  $K$  training examples from each of the categories in both the novel and base datasets. Hence, the entire training process can be simply expressed as follows:

$$\mathcal{M}_{\text{init}} \xrightarrow[e=1 \dots E]{\mathcal{D}_{\text{meta}}^e \subset \mathcal{D}_{\text{base}}} \mathcal{M}_{\text{base}} \xrightarrow{\mathcal{D}_{\text{finertuning}}} \mathcal{M}_{\text{final}}. \quad (1)$$

In the phase of few-shot evaluation, the final model  $\mathcal{M}_{\text{final}}$  is applied to test datasets that contain objects from both the novel and base categories. Fig. 2 provides a visual representation of this process.

### B. Strong Baseline

The existing few-shot object detection algorithms [6, 8] are built upon Faster-RCNN [7] which uses the backbone’s C4 layer features for detection. Compared with generic object detection, objects in RSIs often experience a larger variation in scale. Thus, we are motivated to incorporate multi-level feature extraction to account for the scale variation. Specifically, we incorporate the feature pyramid network (FPN) [9] to allow detection at different scales. In prior works [6][8], the sizes of the query feature and support feature are both resized to  $1 \times 1$  for element-wise multiplication. In our case, we only process the support feature to  $1 \times 1$  size while keeping the query feature unchanged so that the ROI head can obtain more information to identify the objects. Then depth-wise convolution is used to do aggregation operation. The number of

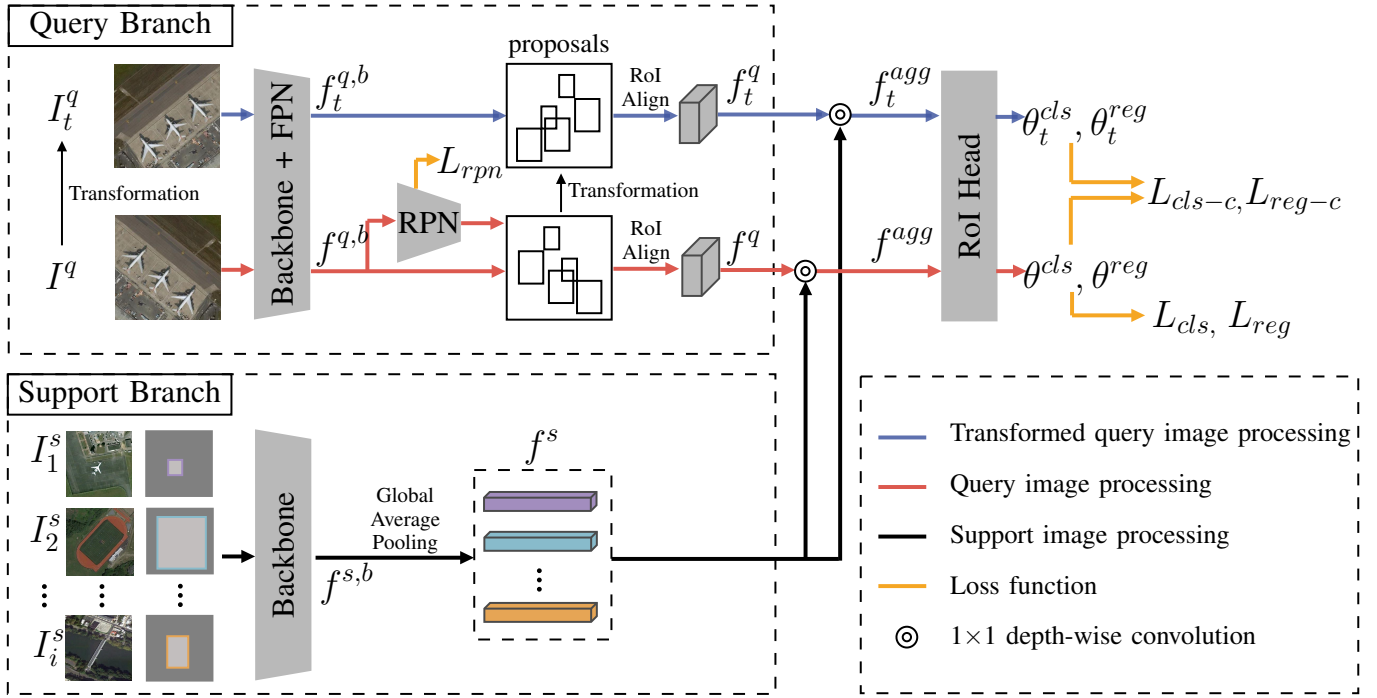


Fig. 3. The overall architecture of TINet.  $I^q$  and its transformed version  $I_t^q$  are fed into a shared backbone network and FPN to obtain query feature map  $f^{q,b}$  and  $f_t^{q,b}$ . After subsequent processing, such as proposal generation by region proposal network (RPN) and the RoI Align,  $f^{q,b}$  and  $f_t^{q,b}$  are aggregated with the support feature  $f^s$ , which is generated by the support branch. The aggregated features  $f_t^{agg}$  and  $f^{agg}$  are fed to the RoI Head to obtain regression parameters ( $\theta_t^{reg}$  and  $\theta^{reg}$ ) and classification scores ( $\theta_t^{cls}$  and  $\theta^{cls}$ ). The supervision loss of the entire network consists of the consistency loss ( $L_{cls-c}$ ,  $L_{reg-c}$ ) and the losses of the Faster-RCNN ( $L_{rpn}$ ,  $L_{cls}$  and  $L_{reg}$ ). Images are from the NWPU VHR-10.v2 dataset.

channels of feature maps is 256 while the channels of feature maps in Meta-RCNN [6] is 1024. During the test phase, we increase the IoU threshold in the non-maximum suppression (NMS) step of the region proposal network (RPN) from 0.7 to 0.9, which helps to prevent the deletion of more bounding boxes due to mistakes, particularly for novel categories. Our experimental results demonstrate that our proposed Strong Baseline outperforms previous meta-learning approaches for remote sensing object detection.

### C. Transformation-Invariant Network

In this section, we further present the proposed transformation-invariant few-shot object detection network (TINet). The overall architecture of the proposed method TINet is shown in Fig. 3. The proposed TINet consists of two branches, namely the query and support branches. The support branch takes the N-way K-shot support images as input and output prototype features for each of the N classes during both the base training and fine-tuning stages. The query branch randomly samples from query images in the base training phase. In the fine-tuning stage, the query branch samples from the N-way K-shot support images as input. For both base training and fine-tuning stages, we maintain the two branches. For testing, we only evaluate using the fine-tuned model. In the following, we explain in detail the query branch, support branch, feature aggregation, and loss designs.

1) *Query branch*: Given a query image  $I^q \in \mathbb{R}^{C \times H \times W}$ , we first produce its transformed version  $I_t^q \in \mathbb{R}^{C \times H \times W}$ . Then,

we feed  $I^q$  and  $I_t^q$  into a shared backbone network and FPN to obtain feature maps  $f^{q,b}$  and  $f_t^{q,b}$ . To ensure the consistency of the generated proposals, we only use  $f^{q,b}$  as the input of the region proposal network (RPN). The same transformation is also applied to generate transformed proposals for  $I_t^q$ . Then, the RoI features  $f^q \in \mathbb{R}^{C_q \times H_q \times W_q}$  and  $f_t^q \in \mathbb{R}^{C_q \times H_q \times W_q}$  of  $I^q$  and  $I_t^q$  can be extracted by an RoI Align operation, where  $H_q$  and  $W_q$  are both set to 7.

2) *Support branch*: We use 4-channel N-way K-shot support images  $I_i^s$  as input for the support branch, where  $i \in \{1, \dots, N\}$ . Specifically, every image  $I_i^s$  includes an RGB image and its binary mask derived from the object bounding box. To ease the computational burden, we resize the spatial size of the object inputs into  $224 \times 224$ . Then, we feed all the support images to the backbone network to obtain feature map  $f^{s,b} \in \mathbb{R}^{C_s \times 224/r \times 224/r}$ , where  $r$  is the stride of the backbone network. It is noteworthy that the backbone of this branch is shared with the query branch except for the first convolution layer. After global average pooling (GAP), we can obtain the final support feature maps  $f^s \in \mathbb{R}^{C_s \times H_s \times W_s}$ , where  $H_s$  and  $W_s$  are both set to 1. If the K is more than 1, the  $f^s$  is the average of the features extracted from K-shot objects.

3) *Feature aggregation*: In our case, we only use the  $1 \times 1$  depth-wise convolution to do aggregation, which is simple but effective. Specifically, the support feature  $f^s \in \mathbb{R}^{C_s \times H_s \times W_s}$  is regarded as a convolution kernel of  $1 \times 1$  depth-wise convolution. The support feature during training is randomly selected from the N-way K-shot support images, and during testing, all the support features must participate to provide the

support feature  $f^s$ . Then, the aggregated features  $f^{agg}$  and  $f_t^{agg}$  are fed to the RoI Head to obtain classification scores  $\theta^{cls}$  and  $\theta_t^{cls}$  and regression parameters  $\theta^{reg}$  and  $\theta_t^{reg}$ .

4) *Consistency loss*: By minimizing the consistency loss, the network can perform consistency detection results on both the original image and its transformed version. Because object detection consists of two sub-tasks (classification and regression), it can be divided into two parts, i.e, classification consistency loss  $L_{cls-c}$  and regression consistency loss  $L_{reg-c}$ . We denote the classification distribution for the  $j$ -th proposal in  $\theta^{cls}$  and  $\theta_t^{cls}$  by  $\sigma^j$  and  $\sigma_t^j$ , respectively. To measure the distance between these two distributions,  $L_2$  loss, Jensen–Shannon divergence (JSD), and Kullback–Leibler divergence (KLD) are popular metrics. Here, we experimentally observe that the  $L_2$  loss performs best. Hence, the classification consistency loss is given as follows:

$$L_{cls-c} = \sum_{j=1}^J \|\sigma^j - \sigma_t^j\|^2 \quad (2)$$

Unlike the classification distribution, regression parameters will change as the image is transformed. We denote the regression results for the  $j$ -th proposal in  $\theta^{reg}$  by  $[\Delta x^j, \Delta y^j, \Delta w^j, \Delta h^j]$ , which represent the offset of the center point and the scale coefficients of width and height. Likewise, we use  $[\Delta x_t^j, \Delta y_t^j, \Delta w_t^j, \Delta h_t^j]$  to present the  $j$ -th parameters in  $\theta_t^{reg}$ . In this paper, we discuss the effect of the three flipping transformations: horizontal flipping, vertical flipping, and diagonal flipping. Since the flipping transformation makes  $\Delta x_t^j$  or  $\Delta y_t^j$  move in the opposite direction, a negative operation should be applied to correct it. Taking diagonal flipping as an example,  $\Delta x^j$  and  $\Delta y^j$  should correspond to  $-\Delta x_t^j$  and  $-\Delta y_t^j$ . Hence, the regression consistency loss using  $L_2$  regularization can be defined as:

$$L_{reg-c} = \frac{1}{4} \sum_{j=1}^J \left[ \left\| \Delta x^j - (-\Delta x_t^j) \right\|^2 + \left\| \Delta y^j - (-\Delta y_t^j) \right\|^2 + \left\| \Delta w^j - \Delta w_t^j \right\|^2 + \left\| \Delta h^j - \Delta h_t^j \right\|^2 \right] \quad (3)$$

For the other two flipping transformations,  $\Delta x^j$  and  $\Delta y^j$  should correspond to  $-\Delta x_t^j$  and  $\Delta y_t^j$  for horizontal flipping and  $\Delta x_t^j$  and  $-\Delta y_t^j$  for vertical flipping.

5) *Total loss*: We finally optimize the total loss  $L_T$  combining the standard supervised losses terms and the consistency losses as below,

$$L_T = \lambda_1 L_{rpn} + \lambda_2 L_{cls} + \lambda_3 L_{reg} + \lambda_4 L_{cls-c} + \lambda_5 L_{reg-c} \quad (4)$$

We empirically set  $\lambda_1 = 1.0$ ,  $\lambda_2 = 1.0$  and  $\lambda_3 = 1.0$ .  $L_{rpn}$ ,  $L_{cls}$  and  $L_{reg}$  represent losses (cross entropy loss and L1 loss) for RPN are the classification loss (cross-entropy loss) and regression loss (L1 loss) for the original query image, respectively.  $\lambda_4$  and  $\lambda_5$  control the strength in transformation consistency. Since object detection consistency is not stable in the early training stage, we choose relatively smaller weights as  $\lambda_4 = 0.05$  and  $\lambda_5 = 0.02$ .

## D. Training and Testing Algorithms

As mentioned in the previous section, the training and testing of our method are slightly different. Therefore, we use two algorithms to provide the detailed process of training and testing. In Alg. (1), we only show how to compute the consistency loss. In both the base training phase and the few-shot fine-tuning phase, consistency loss is used. The testing phase is shown in Alg. (2). What needs to be distinguished is that for the aggregation operation, the support feature during training is randomly selected, and during testing, all the support features must participate. During the testing phase, the transformed images are not included in the testing, so there is no impact on the inference time. The effect of different components in consistency loss on training and testing time can be seen in Section IV-D7.

---

### Algorithm 1 Consistency loss computation

---

**Input:** Query image  $I^q$  and its transformed version  $I_t^q$  support images  $I_1^s, \dots, I_i^s$ .

**Output:** Consistency loss  $L_{reg-c}$ ,  $L_{cls-c}$ .

**Query Branch:**

- 1: Feed  $I^q$  and  $I_t^q$  to the shared backbone and FPN to obtain output features  $f^{q,b}$  and  $f_t^{q,b}$ ;
- 2: Generate proposals using  $f^{q,b}$  by RPN and obtain the flipped proposals;
- 3: Extract query box feature  $f_t^q$  and  $f^q$  by RoI Align.

**Support Branch:**

- 4: Feed  $I_1^s, \dots, I_i^s$  to the shared backbone to obtain output feature  $f_1^{s,b}, \dots, f_i^{s,b}$ ;
  - 5: Generate support features  $f^s$  by GAP;
  - 6: Random sample a support feature  $f_r^s$  from  $f^s$ .
  - 7:  $f_t^{agg} \leftarrow f_t^q \otimes f_r^s$ ;  $f^{agg} \leftarrow f^q \otimes f_r^s$ ;
  - 8: Feed  $f_t^{agg}$  and  $f^{agg}$  to RoI head to obtain  $\theta^{cls}$  and  $\theta^{reg}$ ,  $\theta_t^{cls}$  and  $\theta_t^{reg}$ ;
  - 9: Compute  $L_{cls-c}$  according to Eq. (2) and  $L_{reg-c}$  according to Eq. (3).
- 

---

### Algorithm 2 The overall test procedure (one image)

---

**Input:** Query image  $I^q$  and support images  $I_1^s, \dots, I_i^s$ .

**Output:** Classification score  $\theta^{cls}$ , regression parameters  $\theta^{reg}$ .

**Query Branch:**

- 1: Feed  $I^q$  to the shared backbone and FPN to obtain output feature  $f^{q,b}$ ;
- 2: Generate proposals using  $f^{q,b}$  by RPN;
- 3: Extract query box feature  $f^q$  by RoI Align.

**Support Branch:**

- 4: Feed  $I_1^s, \dots, I_i^s$  to shared backbone to obtain output feature  $f_1^{s,b}, \dots, f_i^{s,b}$ ;
  - 5: Generate support features  $f^s$  by GAP.
  - 6: **for**  $i \leftarrow 1$  to  $N$  **do**
  - 7:  $f_i^{agg} \leftarrow f^q \otimes f_i^s$ ;
  - 8: Feed  $f_i^{agg}$  to RoI head to obtain  $\theta_i^{cls}$  and  $\theta_i^{reg}$ .
  - 9: **end for**
-



TABLE I  
DIFFERENT NOVEL/BASE CLASSES SPLIT SETTINGS FOR OUR EXPERIMENTS

Dataset(split)	Novel classes	Base classes
DIOR(split1)	airplane, baseball field, train station, tennis court, windmill	rest
DIOR(split2)	airplane, airport, expressway toll station, harbor, ground track field	rest
HRRSD	airplane, baseball diamond, ground track field, storage tank	rest
NWPU VHR-10.v2	airplane, baseball diamond, tennis court	rest

TABLE II

COMPARING RESULTS OF DIFFERENT FEW-SHOT OBJECT DETECTION METHODS ON THE DIOR TEST SET IN SPLIT1 (NAP/BAP/MAP). COLORED RESULTS REPRESENT THE **BEST** AND **SECOND-BEST**. \* INDICATES RESULTS REPORTED IN [27], # INDICATES RESULTS REPORTED IN [31]

Method	Backbone	Combination	5-shot			10-shot			20-shot			30-shot		
			nAP	bAP	mAP	nAP	bAP	mAP	nAP	bAP	mAP	nAP	bAP	mAP
FRCN-ft [7]	ResNet-50	FPN	15.9	33.7	29.3	20.4	43.4	37.7	24.8	49.4	43.2	26.5	50.7	44.7
FsDetView [8]	ResNet-50	C4	17.0	37.8	32.6	21.9	39.7	35.3	24.9	41.8	37.6	27.6	46.7	41.9
TFA [22]	ResNet-50	FPN	19.4	36.1	31.9	23.3	40.9	36.5	30.1	48.6	43.9	34.0	50.3	46.2
FSCE [23]	ResNet-50	FPN	20.3	38.0	33.6	26.2	43.5	39.1	34.0	49.6	45.7	37.2	53.4	49.3
Meta-RCNN [6]	ResNet-50	C4	20.7	47.1	40.5	24.7	46.7	41.3	27.9	48.1	43.0	30.0	49.3	44.5
RepMet* [43]	InceptionV3	-	8.0	-	-	14.0	-	-	16.0	-	-	-	-	-
FSRW* [19]	Darknet-19	-	22.0	-	-	28.0	-	-	34.0	-	-	-	-	-
FSODM* [27]	Darknet-53	-	25.0	-	-	32.0	-	-	36.0	-	-	-	-	-
Zhang et al.# [31]	ResNet-101	FPN	<b>34.0</b>	-	-	<b>37.0</b>	-	-	<b>42.0</b>	-	-	-	-	-
Strong Baseline (Ours)	ResNet-50	FPN	22.0	48.0	41.5	26.9	52.1	45.8	32.1	55.5	49.6	36.8	55.4	50.7
TINet (Ours)	ResNet-50	FPN	<b>29.5</b>	<b>56.2</b>	<b>49.5</b>	<b>35.2</b>	<b>56.8</b>	<b>51.4</b>	<b>41.6</b>	<b>59.8</b>	<b>55.3</b>	<b>42.8</b>	<b>62.6</b>	<b>57.7</b>
TINet (Ours)	ResNet-101	FPN	28.6	<b>57.8</b>	<b>50.5</b>	<b>38.4</b>	<b>57.4</b>	<b>52.7</b>	<b>43.2</b>	<b>62.1</b>	<b>57.4</b>	<b>44.6</b>	<b>63.6</b>	<b>58.9</b>

TABLE III

COMPARING RESULTS OF DIFFERENT FSOD METHODS ON THE DIOR TEST SET IN SPLIT2 (NAP). COLORED RESULTS REPRESENT THE **BEST** AND **SECOND-BEST**. \* INDICATES RESULTS REPORTED IN [32], # INDICATES RESULTS REPORTED IN [31]

Method	Backbone	5	10	20	30
FRCN-ft [7]	ResNet-50	14.9	17.6	22.8	23.5
FsDetView [8]	ResNet-50	14.2	16.2	19.1	21.9
TFA [22]	ResNet-50	18.0	20.9	23.0	26.4
FSCE [23]	ResNet-50	19.9	22.7	26.9	30.6
Meta-RCNN [6]	ResNet-50	14.1	17.6	21.0	21.2
RepMet* [43]	InceptionV3	5.6	5.9	6.8	6.5
FSRW* [19]	DarkNet-19	7.0	9.0	14.1	14.4
P-CNN* [32]	ResNet-101	14.9	18.9	22.8	25.7
Zhang et al.# [31]	ResNet-101	15.5	19.7	23.8	29.6
Strong Baseline	ResNet-50	20.1	23.3	26.5	28.1
TINet	ResNet-50	<b>21.7</b>	<b>24.1</b>	<b>28.0</b>	<b>31.9</b>
TINet	ResNet-101	<b>22.8</b>	<b>25.1</b>	<b>29.4</b>	<b>33.2</b>

## IV. EXPERIMENTS

### A. Dataset and Experimental Setting

We conduct experiments on three extensively used remote sensing datasets, i.e., NWPU VHR-10.v2 [11], DIOR [5] and HRRSD [10]. NWPU VHR-10.v2 contains 1172 annotated images distributed into ten categories, which are divided into 75% for training and 25% for testing. For the DIOR dataset, 11,725 images are used as the training set, and the remaining 11,738 images are employed as the test set. Likewise, the HRRSD data are divided into three parts (the training, validation, and test sets), with 5,401, 5,417, and 10,913 images,

respectively.

To establish the few-shot learning setup, we further divide each dataset into two parts, the novel class and the base class following the practice adopted in [27][32]. A detailed split setting is presented in Tab. I. It should be noted that the number of shots denotes the number of instances that are not images because one image contains several instances. We evaluate the testing images, which contain both base and novel classes.

For all the experiments implemented based on our proposed detector, we employ ResNet [44] pre-trained on ImageNet as a backbone network. During the training process, we use an SGD optimizer with a momentum coefficient of 0.9 and a weight decay of 0.0001. The batch size we set for all the datasets is 4. In the base training stage, we set the initial learning rate to 0.01, and the learning rate decreases by 0.1 at 80% of the total iterations. In the few-shot fine-tuning stage, we set the initial learning rate to 0.001, and the learning rate is multiplied by 0.1 at 80% of the total iterations. For NWPU VHR-10.v2, we train 9,000 iterations for base training and 3,000 iterations for few-shot fine-tuning training. For HRRSD and DIOR, we train 36,000 iterations for base training and 6,000 iterations for few-shot fine-tuning training. Moreover, we apply multiscale training and random flipping to enhance the detection performance. The scale range of the input images varies (440, 472, 504, 536, 568, 600). We perform the experiments under the PyTorch framework on a PC with an Intel single-core i7 CPU and a GeForce RTX 3090 GPU.

In the following experimental results, we adopt the method following the evaluation protocol PASCAL visual object classes (VOC) [45]. mAP represents the mean average pre-

TABLE IV

COMPARISON RESULT OF DIFFERENT FEW-SHOT OBJECT DETECTION METHODS ON HRRSD TEST SET (NAP/BAP/MAP). COLORED RESULTS REPRESENT THE BEST AND SECOND-BEST.

Method	Backbone	Combination	5-shot			10-shot			20-shot			30-shot		
			nAP	bAP	mAP	nAP	bAP	mAP	nAP	bAP	mAP	nAP	bAP	mAP
FRCN-ft [7]	ResNet-50	FPN	26.9	79.4	63.3	38.1	80.8	67.7	44.0	82.1	70.4	46.2	82.9	71.6
FsDetView [8]	ResNet-50	C4	35.6	62.2	54.0	42.0	67.8	59.8	48.1	69.8	63.1	52.8	70.0	64.7
TFA [22]	ResNet-50	FPN	36.0	75.3	63.2	45.1	79.3	68.8	51.4	80.7	71.7	53.0	81.0	72.4
FSCE [23]	ResNet-50	FPN	37.5	75.7	64.0	46.3	79.8	69.5	54.5	80.9	72.8	61.9	80.6	74.9
Meta-RCNN [6]	ResNet-50	C4	30.5	71.1	58.6	41.1	73.2	63.3	47.7	73.7	65.7	51.5	75.5	68.1
Strong Baseline	ResNet-50	FPN	32.3	71.2	59.2	43.7	75.4	65.6	53.3	75.1	68.4	61.4	77.2	72.3
TINet	ResNet-50	FPN	38.3	81.8	68.4	47.3	80.2	70.4	58.9	80.5	73.9	64.3	80.8	75.3

TABLE V

COMPARISON RESULT OF DIFFERENT FSOD METHODS ON NWPU VHR-10.v2 TEST SET (NAP). COLORED RESULTS REPRESENT THE BEST AND SECOND-BEST. \* REPRESENTS RESULTS REPORTED IN [33].

Method	Backbone	2	3	5	10
FRCN-ft [7]	ResNet-50	35.1	44.8	48.9	57.3
FsDetView [8]	ResNet-50	40.8	52.2	58.6	65.2
TFA [22]	ResNet-50	42.8	50.7	53.1	60.5
FSCE [23]	ResNet-50	53.4	56.4	60.6	68.7
Meta-RCNN [6]	ResNet-50	43.1	50.6	55.1	62.6
OFA* [33]	ResNet-101	34.0	43.2	60.4	66.7
Strong Baseline	ResNet-50	45.8	55.1	59.8	64.0
TINet	ResNet-50	53.7	55.8	63.5	71.8

cision of all the categories of objects, including the base categories and novel categories. The novel class average precision (nAP) indicates the mean average precision for the novel categories and base class average precision (bAP) indicates the mean average precision for the base categories.

### B. Reproducing Generic FSOD Methods

To make a fair comparison, we first reproduce several state-of-the-art generic few-shot object detection methods based on the open-source framework MMFewShot [46] which is tailored for few-shot learning. These include FRCN-ft[7], TFA[22], FSCE[23], Meta-RCNN [6] and FsDetView[8], and finally, we implemented the proposed Strong Baseline and our TINet. Specifically, the Strong Baseline is referred to in Section III-B. FRCN-ft only uses base class objects to train the Faster-RCNN with FPN in the first phase and then uses combinations of the base class and novel class objects to fine-tune in the second phase. For TFA, we only freeze the backbone in the fine-tuning phase because we can obtain better results in this way, which is slightly different from the original paper. For FSCE, Meta-RCNN, and FsDetView, we keep the same setting as the original paper.

### C. Few-Shot Object Detection Results

1) *DIOR*: We present the results of different methods for split1 and split2 in Tab. II and Tab. III respectively. In split1, as shown in Tab. II, in addition to the reproduced generic few-shot object detection methods, we further incorporate comparisons with RepMet [43] with InceptionV3 [47] as the backbone

and FSRW with DarkNet-19 [48] as backbone according to [27]. We make the following observations from the results. First, the TINet outperforms all competing methods except for nAP@5shot. The gap is particularly significant compared with generic FSOD methods where more than 10% improvements in nAP/bAP/mAP are observed throughout 5 to 30 shots. This suggests the strong few-shot learning capability of TINet. Second, all the transfer-learning approaches and meta-learning approaches outperform the original fine-tuned Faster-RCNN (FRCN-ft). For the meta-learning approaches, we observe that Meta-RCNN and FsDetView only use the C4 layer for subsequent processing, thus they perform relatively worse compared with the Strong Baseline on the DIOR dataset which features large diversity in object scales. For the transfer-learning-based approaches, both FSCE and TFA are way behind TINet despite all are using FPN, probably due to the large intra-class variation in the DIOR dataset. Finally, compared with the results reported by the state-of-the-art methods in RSIs [27][31], we also demonstrate a competitive result, except for the nAP@5 shots. We further present the comparisons for split2 in Tab. III, which is generally considered to be more challenging than split1. Under split2, we observe more significant improvements in TINet from the best-performing methods. These results again validate the effectiveness of the proposed method.

2) *HRRSD*: The quantitative results of applying the different methods to the The HRRSD dataset is shown in Table IV. There is no algorithm tested on HRRSD thus far, so we only make comparisons with the algorithm we implemented. It can be observed that most methods achieve good results because this dataset is not as complex as the DIOR dataset and has fewer object categories. Transfer learning approaches perform strongly in some aspects, especially FSCE. However, our method still performs better than FSCE in nAP in 5 shots, 10 shots, 20 shots, and 30 shots with improvements of 0.8%, 1.0%, 4.4% and 2.4%, respectively.

3) *NWPU VHR-10.v2*: As shown in Table V, since the NWPU VHR-10.v2 dataset is relatively simple, all the methods achieve relatively good results. It can be observed that our Strong Baseline has higher results than the general meta-learning methods but lower results than the transfer learning approach, FSCE. This is because this dataset is very small and the intra-class similarity is not large. TINet still outperforms FSCE on most metrics. Although OFA [33] improves object

TABLE VI

ABLATION EXPERIMENTS OF STRONG BASELINE ON DIOR TEST SET IN SPLIT1 (NAP). 20 AND 30 MEANS IN THE SETTING OF 20-SHOT AND 30-SHOT, RESPECTIVELY. THE FIRST ROW WITHOUT ANY STRATEGY IS EQUIVALENT TO META-RCNN [6]

FPN	Depth-wise convolution	IoU threshold increasing	20	30
			27.9	30.0
✓			30.5	34.3
✓	✓		31.5	36.0
✓	✓	✓	<b>32.1</b>	<b>36.8</b>

recognition in novel categories by rotating the support samples, increases the inference time, and does not use the oriented feature augmentation method in the base training phase, which may reduce the generalization performance.

D. Ablation Study

We conduct ablation experiments on the DIOR dataset (split1) to reveal the effectiveness of each individual component. Unless otherwise specified, the backbone network chosen is ResNet-50.

1) *Ablation study of Strong Baseline:* We first investigate the effectiveness of including FPN, depth-wise convolution, and IoU thresholding for the Strong Baseline method, with results shown in Tab. VI. The first row without any strategy is equivalent to Meta-RCNN [6]. When FPN is used to replace the C4 layer for subsequent processing, the network performance is greatly improved, suggesting the importance of handling large-scale variation. Depth-wise convolution represents that  $1 \times 1$  depth-wise convolution is used to aggregate  $1 \times 1$  support feature and query feature. This operation increases the results slightly compared with that element-wise multiplication is used to aggregate  $1 \times 1$  support feature and  $1 \times 1$  query feature. Increasing the IoU threshold in the NMS of RPN from 0.7 to 0.9 can further improve performance. In the subsequent experiments, we will use the Strong Baseline as the basic network.

2) *Alternative hyper-parameters of loss  $L_T$ :* General object detectors always focus on two main sub-tasks (regression and classification) so that the weight of auxiliary losses should be relatively smaller. We empirically find  $\lambda_4 = 0.05$  and  $\lambda_5 = 0.02$  on split 2 of DIOR and fix the parameters throughout all experiments. We also carried out additional evaluations on the robustness of the choice of  $\lambda$ s in Tab. VII. In general, stable performance is observed around the hyper-parameters we chose.

3) *Comparison with data augmentation:* There are two consistency losses ( $L_{cls-c}$  and  $L_{reg-c}$ ) in the TINet. As shown in Tab. VIII, we examine the influence of  $L_{cls-c}$  and  $L_{reg-c}$  and make a comparison with data augmentation, which augments the image before feeding it into the query branch. The experimental results in first row are obtained without any strategy. It should be noted that for data augmentation, we choose a combination of horizontal, vertical, and diagonal

TABLE VII

COMPARING DIFFERENT  $\lambda$  ON DIOR TEST SET IN SPLIT1 (NAP) UNDER 20 AND 30 SHOTS.

$\lambda_4$	$\lambda_5$	20	30	$\lambda_4$	$\lambda_5$	20	30
0.05	0.05	42.2	42.1	0.02	0.02	40.9	41.8
0.05	0.02	41.6	42.8	0.02	0.05	41.3	42.4
1	1	16.7	24.8	0.5	0.5	37.7	38.1

TABLE VIII

COMPARISON EXPERIMENTS WITH DATA AUGMENTATION ON DIOR TEST SET IN SPLIT1 (NAP). 5, 10, 20 AND 30 MEANS IN THE SETTING OF 5-SHOT, 10-SHOT, 20-SHOT AND 30-SHOT, RESPECTIVELY. DATA AUG REPRESENTS DATA AUGMENTATION. THE EXPERIMENTAL RESULTS IN FIRST ROW ARE OBTAINED WITHOUT ANY STRATEGY.

Data Aug	$L_{cls-c}$	$L_{reg-c}$	5	10	20	30
			20.8	23.8	30.1	36.3
✓			22.0	26.9	32.1	36.8
	✓		29.1	33.9	40.5	40.9
		✓	27.8	31.8	39.3	41.6
	✓	✓	28.8	34.3	41.1	42.2
✓	✓	✓	<b>29.5</b>	<b>35.2</b>	<b>41.6</b>	<b>42.8</b>

flipping. The consistency loss  $L_{cls-c}$  and  $L_{reg-c}$  here are both the  $L_2$  loss, and the corresponding flipping method is diagonal flipping. It can be seen that data augmentation improves the performance of the network, but as the number of shots increases, the effect decreases significantly. Adding only a consistency loss  $L_{cls-c}$  and  $L_{reg-c}$  is better than adding data augmentation. The addition of both of the  $L_{cls-c}$  or  $L_{reg-c}$  can make the network obtain stable improvements except in 5-shot. The best result is achieved when consistency loss and data augmentation are added simultaneously, which also shows that consistency loss and data augmentation are complementary to each other.

4) *Alternative transformations:* We verify the effect of the different flipping transformations on the experimental results. As shown in Tab. IX, we observe similar results for both the horizontal and vertical flips. The result of the diagonal flip is slightly better than the previous two. This is because the diagonal flip introduces fewer changes to the object’s appearance so that the training is more stable compared to the horizontal and vertical flips.

5) *Alternative consistency regularizations.:* We verify the effect of different regularizations in the classification consistency loss  $L_{con-c}$  on the results. As shown in Tab. X, the JSD and KLD represents Jensen–Shannon divergence and Kullback–Leibler divergence, respectively. The weight of JSD and KLD here we chose are 0.05 and 0.1. It can be observed that simply using the  $L_2$  loss yields the best results in most metrics except in 5-shot. Because the  $L_2$  loss is more sensitive to outliers, it can play a more restrictive role.

6) *Pearson correlation coefficient:* We further measure the calibration of detection models by the Pearson Correlation Coefficient (PCC), defined as follows:



TABLE IX

DETECTION RESULTS OF ALTERNATIVE TRANSFORMATIONS ON DIOR TEST SET IN SPLIT1 (NAP). 5, 10, 20 AND 30 MEANS IN THE SETTING OF 5-SHOT, 10-SHOT, 20-SHOT AND 30-SHOT, RESPECTIVELY.

Flipping method	5	10	20	30
None	22.0	26.9	32.1	36.8
Vertical	28.1	34.1	39.1	41.3
Horizontal	28.5	34.5	39.4	41.2
Diagonal	<b>29.5</b>	<b>35.2</b>	<b>41.6</b>	<b>42.8</b>

TABLE X

DETECTION RESULTS WITH ALTERNATIVE CONSISTENCY REGULARIZATIONS ON DIOR TEST SET IN SPLIT1 (NAP). 5, 10, 20, AND 30 MEAN IN THE SETTING OF 5-SHOT, 10-SHOT, 20-SHOT, AND 30-SHOT, RESPECTIVELY.

Regularization method	5	10	20	30
None	22.0	26.9	32.1	36.8
JSD	27.8	34.8	38.1	41.4
KLD	<b>30.3</b>	34.7	37.9	40.2
$L_2$	29.5	<b>35.2</b>	<b>41.6</b>	<b>42.8</b>

$$r = \frac{\sum (x - m_x)(y - m_y)}{\sqrt{\sum (x - m_x)^2 \sum (y - m_y)^2}} \quad (5)$$

$x$  and  $y$  are respectively the IoU between ground-truth and predicted bounding boxes and the confidence score (the highest posterior). A high correlation indicates the confidence is well calibrated.  $m_x$  and  $m_y$  are the mean of the  $x$  and  $y$  respectively. The results (shown in Fig. 4) demonstrate that the TINet obtained a higher value of PCC than the Strong Baseline and Meta-RCNN in all the datasets, suggesting TINet is better calibrated than others.

7) *Training and testing time*: The results are shown in Tab. XI. Here one iteration includes four multi-scale images, and in the testing phase, the images are resized to  $600 \times 600$ . It can be observed that the training time of TINet increases slightly compared with Strong Baseline because TINet has to process two images simultaneously. However, the inference time of all the comparison methods remains the same. In addition, the loss computation has little effect on the time of

TABLE XI

THE COMPARISON OF TRAINING AND TESTING TIME BETWEEN THE STRONG BASELINE AND TINET.

Method	Training (iteration/s)	Testing (frame/s)
Strong Baseline	4.92	15.5
TINet(w/o $L_{cls-c}$ )	4.29	15.5
TINet(w/o $L_{reg-c}$ )	4.35	15.5
TINet	4.27	15.5

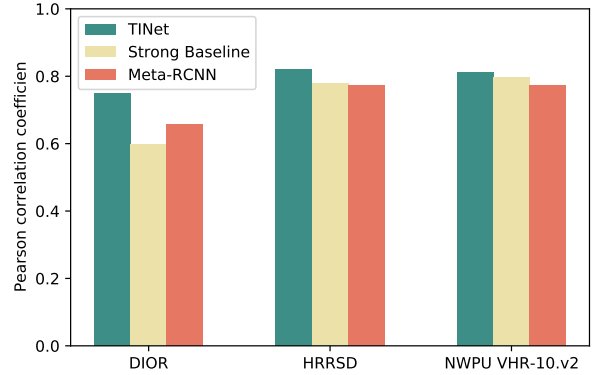


Fig. 4. Pearson correlation coefficient (PCC) between classification scores and IoUs.

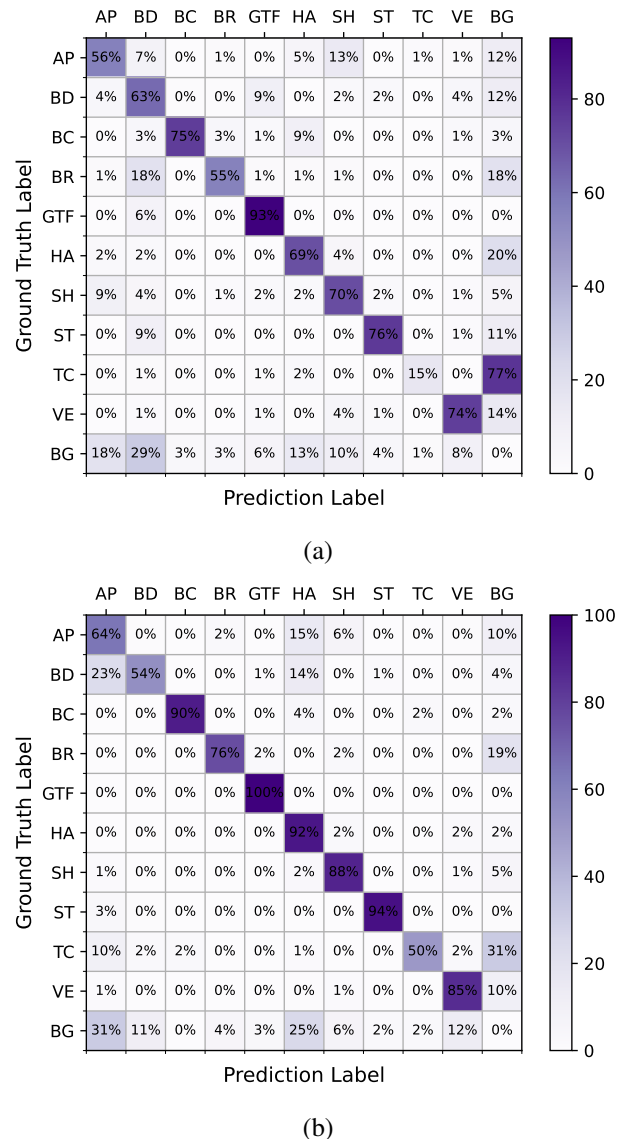


Fig. 5. Comparison of confusion matrix between the Strong Baseline and TINet. (a) Confusion matrix of the Strong Baseline. (b) Confusion matrix of TINet.

network training.

### E. Visualization

To more intuitively demonstrate the effectiveness of our method, we visualize the confusion matrix and prediction results.

1) *Confusion matrix*: We use the detection results of the NWPU VHR-10.v2 test set to generate the confusion matrix. As shown in Fig. 5, the abbreviations for the categories are AP-airplane, BD-baseball diamond, BC-basketball court, BR-bridge, GTF-ground track field, HA-harbour, SH-ship, ST-storage tank, TC-tennis court, VE-vehicle, and BG-background. Different from the classification task, the detection task has cases of false positives and missing detections. Thus, to cover all cases, the background class is necessary. **Note that the percentage sum of the horizontal axis is 100%, while the vertical axis is not 100% because we only normalize the value according to the horizontal axis.** It can be observed that the novel class (AP, BD, and TC) of the Strong Baseline has a low probability of being recognized correctly. Our method alleviates this problem to some extent. In addition, it is worth mentioning that our method does not forget the characteristics of the base class while training on the novel class.

2) *Prediction results*: As shown in Fig. 6), We present a comparison of several Few-Shot Object Detection (FSOD) methods on the DIOR dataset of 30-shot at split1, which contains objects of the novel category, including airplanes, baseball fields, train stations, tennis courts, and windmills, as well as a small number of objects from the base category. It can be observed that the proposed method TINet has a strong generalization ability due to its multi-scale feature structure and transformation invariant learning. Interestingly, for small objects such as airplanes and windmills, the Meta-RCNN without the FPN structure performs even worse than the original finetuning Faster-RCNN (FRCN-ft). However, the addition of the Strong Baseline greatly improves the detection results of Meta-RCNN, achieving similar performance to FSCE. Furthermore, by incorporating a transformation invariant strategy on top of the Strong Baseline, the TINet further enhances the detection performance for objects with different orientations, such as airplanes and tennis courts. For the simpler objects, such as baseball fields without scale and orientation diversity, all the compared algorithms achieve comparable detection results. Overall, our TINet produces the best detection results compared with all competing methods. In addition, we provide more qualitative results with both novel and base objects on the HRRSD (30-shot) dataset in Fig. 7. This dataset is simpler than DIOR, resulting in fewer false detections.

## V. CONCLUSION

In this paper, in light of the challenges in few-shot object detection (FSOD) for remote sensing images (RSIs), we first propose to modify from existing meta-learning-based FSOD method by incorporating FPN and feature fusion. To improve the network's ability to learn from unlabeled samples, we further propose to incorporate transformation invariance into

the baseline, which is then referred to as TINet. Extensive experiments demonstrate the effectiveness of our method, and the method achieved state-of-the-art performances on the vast majority of the metrics on three widely used optical remote sensing object detection datasets, i.e., NWPU VHR-10.v2, DIOR, and HRRSD. It is worth noting that our work is to demonstrate that the improvement of the FSOD in RSIs by geometric transformation is significant. In general, more geometric transformations may further improve performance, such as arbitrary rotation, scaling, translation, etc, which will be considered in detail in our future work. Among them, arbitrary rotation transformation may introduce an artificial black border area and the risk of GT information leakage, which requires a special design.

## REFERENCES

- [1] X. Yang, J. Yan, Z. Feng, and T. He, "R3det: Refined single-stage detector with feature refinement for rotating object," in *Proceedings of the AAAI conference on artificial intelligence*, 2021.
- [2] N. Liu, T. Celik, T. Zhao, C. Zhang, and H.-C. Li, "Afdet: Toward more accurate and faster object detection in remote sensing images," *IEEE Journal of Selected Topics in Applied Earth Observations and Remote Sensing*, 2021.
- [3] X. Yang, L. Hou, Y. Zhou, W. Wang, and J. Yan, "Dense label encoding for boundary discontinuity free rotation detection," in *Proceedings of the IEEE/CVF Conference on Computer Vision and Pattern Recognition (CVPR)*, 2021.
- [4] Q. Ming, L. Miao, Z. Zhou, X. Yang, and Y. Dong, "Optimization for arbitrary-oriented object detection via representation invariance loss," *IEEE Geoscience and Remote Sensing Letters*, 2022.
- [5] K. Li, G. Wan, G. Cheng, L. Meng, and J. Han, "Object detection in optical remote sensing images: A survey and a new benchmark," *ISPRS Journal of Photogrammetry and Remote Sensing*, 2020.
- [6] X. Yan, Z. Chen, A. Xu, X. Wang, X. Liang, and L. Lin, "Meta r-cnn: Towards general solver for instance-level low-shot learning," in *Proceedings of the IEEE/CVF International Conference on Computer Vision*, 2019.
- [7] S. Ren, K. He, R. Girshick, and J. Sun, "Faster r-cnn: Towards real-time object detection with region proposal networks," *Advances in neural information processing systems*, 2015.
- [8] Y. Xiao and R. Marlet, "Few-shot object detection and view-point estimation for objects in the wild," in *European conference on computer vision*, 2020.
- [9] T.-Y. Lin, P. Dollár, R. Girshick, K. He, B. Hariharan, and S. Belongie, "Feature pyramid networks for object detection," in *Proceedings of the IEEE conference on computer vision and pattern recognition*, 2017.
- [10] Y. Zhang, Y. Yuan, Y. Feng, and X. Lu, "Hierarchical and robust convolutional neural network for very high-resolution remote sensing object detection," *IEEE Transactions on Geoscience and Remote Sensing*, 2019.
- [11] K. Li, G. Cheng, S. Bu, and X. You, "Rotation-insensitive and context-augmented object detection in remote sensing images," *IEEE Transactions on Geoscience and Remote Sensing*, 2017.
- [12] G. Cheng, Y. Si, H. Hong, X. Yao, and L. Guo, "Cross-scale feature fusion for object detection in optical remote sensing images," *IEEE Geoscience and Remote Sensing Letters*, 2021.
- [13] N. Liu, T. Celik, and H.-C. Li, "Gated ladder-shaped feature pyramid network for object detection in optical remote sensing images," *IEEE Geoscience and Remote Sensing Letters*, 2022.
- [14] P. Wang, X. Sun, W. Diao, and K. Fu, "Fmssd: Feature-merged single-shot detection for multiscale objects in large-scale re-



Fig. 6. Detection results of different methods of sample images including the detected novel objects and a small number of base objects on DIOR dataset (30-shot at split1).



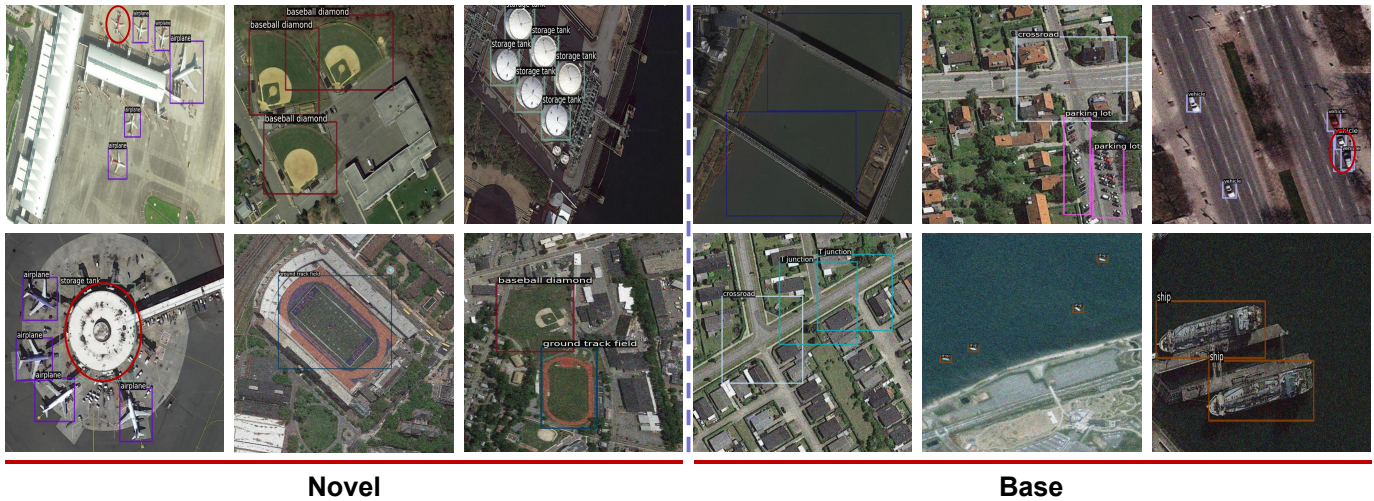


Fig. 7. Detection results of the TINet for the novel and base objects in HRRSD dataset (30-shot). Objects of different categories are represented by rectangular boxes of different colors. Failure cases are represented by red ellipses.

remote sensing imagery,” *IEEE Transactions on Geoscience and Remote Sensing*, 2020.

[15] W. Ma, N. Li, H. Zhu, L. Jiao, X. Tang, Y. Guo, and B. Hou, “Feature split-merge-enhancement network for remote sensing object detection,” *IEEE Transactions on Geoscience and Remote Sensing*, 2022.

[16] J. Han, J. Ding, J. Li, and G.-S. Xia, “Align deep features for oriented object detection,” *IEEE Transactions on Geoscience and Remote Sensing*, 2022.

[17] X. Yang and J. Yan, “Arbitrary-oriented object detection with circular smooth label,” *European Conference on Computer Vision (ECCV)*, 2020.

[18] B. Sun, B. Li, S. Cai, Y. Yuan, and C. Zhang, “Fsce: Few-shot object detection via contrastive proposal encoding,” in *Proceedings of the IEEE/CVF Conference on Computer Vision and Pattern Recognition*, 2021.

[19] B. Kang, Z. Liu, X. Wang, F. Yu, J. Feng, and T. Darrell, “Few-shot object detection via feature reweighting,” in *Proceedings of the IEEE/CVF International Conference on Computer Vision*, 2019.

[20] Q. Fan, W. Zhuo, C.-K. Tang, and Y.-W. Tai, “Few-shot object detection with attention-rpn and multi-relation detector,” in *Proceedings of the IEEE/CVF Conference on Computer Vision and Pattern Recognition*, 2020.

[21] A. Li and Z. Li, “Transformation invariant few-shot object detection,” in *Proceedings of the IEEE/CVF Conference on Computer Vision and Pattern Recognition*, 2021.

[22] X. Wang, T. E. Huang, T. Darrell, J. E. Gonzalez, and F. Yu, “Frustratingly simple few-shot object detection,” 2020.

[23] B. Sun, B. Li, S. Cai, Y. Yuan, and C. Zhang, “Fsce: Few-shot object detection via contrastive proposal encoding,” in *Proceedings of the IEEE conference on computer vision and pattern recognition (CVPR)*, 2021.

[24] J. Wu, S. Liu, D. Huang, and Y. Wang, “Multi-scale positive sample refinement for few-shot object detection,” in *European Conference on Computer Vision*, 2020.

[25] L. Qiao, Y. Zhao, Z. Li, X. Qiu, J. Wu, and C. Zhang, “Defrcn: Decoupled faster r-cnn for few-shot object detection,” in *Proceedings of the IEEE/CVF International Conference on Computer Vision*, 2021.

[26] K. Guirguis, A. Hendawy, G. Eskandar, M. Abdelsamad, M. Kayser, and J. Beyerer, “Cfa: Constraint-based finetuning approach for generalized few-shot object detection,” in *Proceedings of the IEEE/CVF Conference on Computer Vision and Pattern Recognition*, 2022.

[27] X. Li, J. Deng, and Y. Fang, “Few-shot object detection on remote sensing images,” *IEEE Transactions on Geoscience and Remote Sensing*, 2022.

[28] Z. Zhao, P. Tang, L. Zhao, and Z. Zhang, “Few-shot object detection of remote sensing images via two-stage fine-tuning,” *IEEE Geoscience and Remote Sensing Letters*, 2022.

[29] Y. Zhou, H. Hu, J. Zhao, H. Zhu, R. Yao, and W.-L. Du, “Few-shot object detection via context-aware aggregation for remote sensing images,” *IEEE Geoscience and Remote Sensing Letters*, 2022.

[30] Z. Xiao, J. Qi, W. Xue, and P. Zhong, “Few-shot object detection with self-adaptive attention network for remote sensing images,” *IEEE Journal of Selected Topics in Applied Earth Observations and Remote Sensing*, 2021.

[31] Y. Zhang, B. Zhang, and B. Wang, “Few-shot object detection with self-adaptive global similarity and two-way foreground stimulator in remote sensing images,” *IEEE Journal of Selected Topics in Applied Earth Observations and Remote Sensing*, 2022.

[32] G. Cheng, B. Yan, P. Shi, K. Li, X. Yao, L. Guo, and J. Han, “Prototype-cnn for few-shot object detection in remote sensing images,” *IEEE Transactions on Geoscience and Remote Sensing*, 2022.

[33] Z. Zhang, J. Hao, C. Pan, and G. Ji, “Oriented feature augmentation,” 2021.

[34] A. Tarvainen and H. Valpola, “Mean teachers are better role models: Weight-averaged consistency targets improve semi-supervised deep learning results,” *Advances in neural information processing systems*, 2017.

[35] K. Sohn, D. Berthelot, N. Carlini, Z. Zhang, H. Zhang, C. A. Raffel, E. D. Cubuk, A. Kurakin, and C.-L. Li, “Fixmatch: Simplifying semi-supervised learning with consistency and confidence,” 2020.

[36] S. Laine and T. Aila, “Temporal ensembling for semi-supervised learning,” in *International Conference on Learning Representations*, 2017.

[37] T. Miyato, S.-i. Maeda, M. Koyama, and S. Ishii, “Virtual adversarial training: a regularization method for supervised and semi-supervised learning,” *IEEE transactions on pattern analysis and machine intelligence*, 2018.

[38] X. Xu, M. C. Nguyen, Y. Yazici, K. Lu, H. Min, and C.-S. Foo, “Semicurv: Semi-supervised curvilinear structure segmentation,” *IEEE Transactions on Image Processing*, 2022.

[39] M. Xu, Z. Zhang, H. Hu, J. Wang, L. Wang, F. Wei, X. Bai, and Z. Liu, “End-to-end semi-supervised object detection with

- soft teacher,” in *Proceedings of the IEEE/CVF International Conference on Computer Vision*, 2021.
- [40] X. Feng, X. Yao, G. Cheng, and J. Han, “Weakly supervised rotation-invariant aerial object detection network,” in *Proceedings of the IEEE/CVF Conference on Computer Vision and Pattern Recognition*, 2022.
- [41] X. Feng, X. Yao, G. Cheng, J. Han, and J. Han, “Saenet: Self-supervised adversarial and equivariant network for weakly supervised object detection in remote sensing images,” *IEEE Transactions on Geoscience and Remote Sensing*, 2021.
- [42] X. Xu and G. H. Lee, “Weakly supervised semantic point cloud segmentation: Towards 10x fewer labels,” in *Proceedings of the IEEE/CVF conference on computer vision and pattern recognition*, 2020.
- [43] L. Karlinsky, J. Shtok, S. Harary, E. Schwartz, A. Aides, R. Feris, R. Giryes, and A. M. Bronstein, “Repmet: Representative-based metric learning for classification and few-shot object detection,” in *Proceedings of the IEEE/CVF conference on computer vision and pattern recognition*, 2019.
- [44] K. He, X. Zhang, S. Ren, and J. Sun, “Deep residual learning for image recognition,” in *2016 IEEE Conference on Computer Vision and Pattern Recognition (CVPR)*, 2016.
- [45] M. Everingham, L. V. Gool, C. Williams, J. Winn, and A. Zisserman, “The pascal visual object classes (voc) challenge,” *International Journal of Computer Vision*, 2010.
- [46] mmfewshot Contributors, “Openmmlab few shot learning toolbox and benchmark,” <https://github.com/open-mmlab/mmfewshot>, 2021.
- [47] C. Szegedy, V. Vanhoucke, S. Ioffe, J. Shlens, and Z. Wojna, “Rethinking the inception architecture for computer vision,” in *Proceedings of the IEEE conference on computer vision and pattern recognition*, 2016.
- [48] J. Redmon and A. Farhadi, “Yolo9000: better, faster, stronger,” in *Proceedings of the IEEE conference on computer vision and pattern recognition*, 2017.